Journal of Sound and Vibration (1972) **22** (2), 233–246

ACOUSTIC REFRACTION AND ATTENUATION IN CYLINDRICAL AND ANNULAR DUCTS

P. N. SHANKAR

Department of Aerospace Engineering,
University of Maryland, College Park, Maryland 20742, *U.S.A.*

(*Received* 24 *January* 1972)

Previous work has shown that refractive effects in sound propagation can be calculated correctly only by treating the complete boundary value problem. Starting from a given acoustic source pressure distribution the field is to be calculated everywhere. Such a calculation is effected here for cylindrical and annular ducts. The eigenvalue problem resulting from the assumption of complete separability in all the variables is solved numerically for the lowest and the next ten additional eigenvalues β_n and the corresponding eigenfunctions ϕ_n. These eigenfunctions are then combined by a least total error squared method to represent the initial pressure distribution. This procedure leads to the pressure pattern everywhere in the duct.

The calculation of distinct eigenvalues is not entirely straightforward. Some guidance is therefore given as to how the eigenvalues may be located. Among a number of typical calculations, cases with wall admittance are presented. They show clearly that the combined refractive-attenuation effects are indeed complicated. Lowest mode calculations may be very misleading.

1. INTRODUCTION

There has been, during recent years, a renewed interest in the study of sound propagation in moving media contained in ducts. This interest is due chiefly to the emergence of jet engine noise as a major problem. The sound that is generated inside the engine, mainly as pure tone noise, has to propagate through ducts containing the flowing gases. In addition to being convected and possibly attenuated at the walls, the sound waves suffer refraction as a result of the non-uniformity of the flow. Thus initially uniform sound pressure profiles will lead to non-uniform profiles further down the duct. It is this aspect that we wish to consider here.

In an early paper [1], Pridmore-Brown considered the propagation of sound in a shear flow contained between two infinite flat plates. By assuming complete separability in all the independent variables x, y and t, he derived an eigenvalue problem for the modified wave number or propagation constant. The eigenvalue problem was solved approximately for the lowest eigenvalue for particular velocity profiles by a WKB type method. More recently, Mungur and Gladwell [2] solved Pridmore-Brown's eigenvalue problem numerically, again for the lowest modes. This work was then extended [3] to the more practical cylindrical and annular geometries with hard and soft walls.

These studies raise a number of questions. The eigenvalue problem is not of the Sturm–Liouville type: the usual theorems on orthogonality and completeness do not apply, at least in any obvious manner. Clearly, if the eigenfunctions are not complete, they cannot be used to represent a given source pressure distribution. This would imply that the separable solutions are not applicable to the problem. On the other hand even if the eigenfunctions are complete but not orthogonal (to any known weighting function), how does one combine them to represent the source distribution?

It was to avoid these difficulties that the author suggested a perturbation approach to the problem in the limit of weak refraction, where the form of the solution was not assumed

a priori [4]. The complete initial boundary value problem was solved for a uniform source distribution in an arbitrary shear flow. In addition to revealing a number of novel features, the solution clearly indicated the need to consider the complete boundary value problem. In this limit, it was found, the spatial variables did indeed separate. This solution was, however, inadequate at high subsonic Mach numbers and at high frequency, when the refractive effects became substantial.

Recently [5], it was realized that in the absence of a mathematical proof of completeness of the eigenfunctions resulting from Pridmore-Brown's eigenvalue problem, it might still be possible to demonstrate their completeness "experimentally"; the eigenfunctions could then be used to solve the complete boundary value problem for a given source pressure distribution. This was done for the plane case; the eigenfunctions did indeed appear to be complete and in the case of weak shear the solutions appeared to agree with the perturbation calculation. These results, moreover, showed that at high Mach number and frequency a saturation effect limited the actual build up near the walls of the duct. In this paper we wish to demonstrate similar calculations for cylindrical and annular geometries with hard and soft walls. Again we find that the eigenfunctions appear to be complete. The geometrical effects are significant, particularly when the sound waves propagate against the flow.

2. FORMULATION

We consider an axially symmetric geometry (Figure 1) with either a cylindrical passage ($r_i = 0$) or an annular passage ($r_i \neq 0$). For such a geometry with the assumed symmetry, the equations governing sound propagation in an ideal inviscid, non-heat conducting medium are

$$\frac{1}{c^2}\left(\frac{\partial p}{\partial t} + V(r)\frac{\partial p}{\partial z}\right) + \rho_0\left(\frac{\partial u_z}{\partial z} + \frac{\partial u_r}{\partial r} + \frac{u_r}{r}\right) = 0, \tag{1a}$$

$$\frac{\partial u_z}{\partial t} + V(r)\frac{\partial u_z}{\partial z} + u_r\frac{\mathrm{d}V}{\mathrm{d}r} = -\frac{1}{\rho_0}\frac{\partial p}{\partial z}, \tag{1b}$$

$$\frac{\partial u_r}{\partial t} + V(r)\frac{\partial u_r}{\partial z} = -\frac{1}{\rho_0}\frac{\partial p}{\partial r}, \tag{1c}$$

where u_z, u_r and p are first-order acoustic quantities, $V(r)$ is the steady subsonic axial velocity in the duct, ρ_0 is the ambient density and $c = (\gamma RT_0)^{1/2}$ is the ambient sound speed.

Sound is generated at the plane $z = 0$, where the acoustic pressure is given by

$$\begin{aligned} p(r,0,t) &= \hat{p}(r)\cos\omega t \\ &= \mathrm{Re}\{\hat{p}(r)e^{-i\omega t}\}. \end{aligned} \tag{2}$$

In order to calculate the acoustic field everywhere inside the duct we assume separable solutions of the form

$$p(r,z,t) \sim \phi(r)\exp\{ik(\beta z - ct)\}, \tag{3a}$$

$$u_r(r,z,t) \sim f(r)\exp\{ik(\beta z - ct)\}, \tag{3b}$$

$$u_z(r,z,t) \sim g(r)\exp\{ik(\beta z - ct)\}, \tag{3c}$$

where $k = \omega/c$ is the known ambient wave number in the absence of flow and β is an initially unknown "propagation constant". Substitution of these expressions into the governing equations (1a, 1b, 1c) leads to the following equation for ϕ:

$$\frac{\mathrm{d}^2\phi}{\mathrm{d}r^2} + \left[\frac{2\beta\,\mathrm{d}M/\mathrm{d}r}{(1-\beta M)} + \frac{1}{r}\right]\frac{\mathrm{d}\phi}{\mathrm{d}r} + k^2[(1-\beta M)^2 - \beta^2]\phi = 0. \tag{4}$$

If the impedance at the walls is $\hat{z}$, the wall boundary conditions translate to

$$p(r,z,t) = \begin{cases} \hat{z}u_r & \text{at } r = r_o \\ -\hat{z}u_r & \text{at } r = r_i, \end{cases} \tag{5a}$$

or,

$$\frac{d\phi}{dr} - \frac{i\rho_0 ck(1-\beta M)}{(\pm\hat{z})}\phi = 0 \qquad \text{at } r = r_o, r_i. \tag{5b}$$

Note that $M(r) = V(r)/c$ is the Mach number of the axial flow.

The equation (4) together with the boundary conditions (5b) constitutes an eigenvalue problem for β. The eigenvalue β, however, appears in a non-linear fashion in both the coefficients of ϕ and of $d\phi/dr$. We remark once again that this is not a Sturm–Liouville system and the usual theorems on the eigenvalues, on completeness and on orthogonality, do not apply directly. We shall, however, *assume* that: (i) there exists a lowest eigenvalue, β_0, (ii) there exists an infinite set of distinct higher eigenvalues β_n, and (iii) the corresponding eigenfunctions ϕ_n are complete. The plausibility of these assumptions will be demonstrated in what follows.

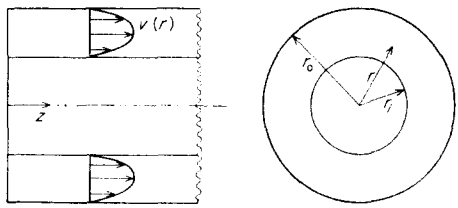

Figure 1. Sound is generated at the plane $z = 0$ and propagates to the right in the semi-infinite duct. $V(r)$ is the axial velocity of the medium. For the annular geometry the gap width $(r_o - r_i)$ is equal to b. For a cylindrical duct the inner cylinder is absent and r_o is equal to b.

The pressure everywhere in the duct is then given by

$$p(r,z,t) = \sum_{n=0}^{\infty} a_n \phi_n(r) \exp\{ik(\beta_n z - ct)\}, \tag{6}$$

where the amplitude coefficients a_n have to be determined from the source pressure distribution $\hat{p}(r)$. For calculational purposes we limit ourselves to the lowest eleven eigenfunctions and the corresponding a_n's are calculated such as to minimize the total error squared over the source pressure profile. These details will be given in the next section.

A comment about the boundary condition (5) is in order. When there is slip at the walls, that is if $M(r) \neq 0$ at the walls, the condition (5) is subject to controversy. It is argued by some that in such cases continuity of particle displacement is the correct condition. In any case, we shall avoid this difficulty by only considering realistic Mach number profiles disallowing slip at the wall.

3. NUMERICAL PROCEDURE

It is convenient to normalize all length scales by the duct gap width $b = (r_0 - r_i)$. For a cylindrical duct the length b is simply the radius of the duct. The eigenvalue problem may then be written as

$$\frac{d^2\phi}{d\bar{r}^2} + \left[\frac{2\beta\, dM/d\bar{r}}{(1-\beta M)} + \frac{1}{\bar{r}}\right]\frac{d\phi}{d\bar{r}} + (kb)^2[(1-\beta M)^2 - \beta^2]\phi = 0 \tag{7a}$$

$$\frac{d\phi}{d\bar{r}} \pm i\eta kb\phi = 0 \qquad \text{at } \bar{r} = \bar{r}_i, \bar{r}_i + 1, \tag{7b}$$

where $\bar{r} = r/b$ is the non-dimensional radius and η is the wall admittance defined by

$$\eta = \rho_0 c/\hat{z}. \tag{8}$$

For cylindrical ducts the inner wall condition is replaced by a finiteness condition, i.e. ϕ has to be finite at $\bar{r} = 0$.

The eigenvalue problem is solved numerically as follows. Values of the frequency parameter kb, the inner radius r_i, and the wall admittance η are chosen and a particular axial Mach number profile $M(\bar{r})$ is selected. Since the normalization is arbitrary the value of $\phi_n(\bar{r})$ at $\bar{r} = \bar{r}_i$ is always chosen as $(1 + i)$ where $i = \sqrt{-1}$. A trial value of β_n is chosen, the boundary condition at the inner wall is satisfied and the differential equation (7a) is integrated numerically by a fourth-order Runge–Kutta scheme. When the outer wall is reached the condition (7b) will not normally be satisfied. The value of β_n is altered suitably and the integration is re-effected. The procedure is repeated until the boundary condition is satisfied to sufficient accuracy.

Now, one needs to find N distinct eigenvalues and eigenfunctions—in our case the lowest eleven ($N = 11$). Thus when an eigenvalue is located one needs to make sure that it is a member of the sequence sought. Guided by the no-flow and uniform flow cases, we use the empirical rule that the real part of the eigenfunction $\phi_n(r)$ has n zeros between $r = r_i$ and $r = r_i + 1$, i.e. between the walls. So far we have found no exception to this rule. On this basis, if the eigenvalue β_n is being sought one checks the zeros of the real part of the located eigenfunction; if the number of zeros is n the eigenfunction is the required one; if not, one repeats the search.

It should be clear that a knowledge of the approximate location of the eigenvalues and of their dependence on the parameters of the problem is of considerable value. For hard-walled ducts the lowest eigenvalue and possibly some of the higher ones are purely real; the corresponding eigenfunctions will then have equal real and imaginary parts. For soft-walled ducts all the eigenvalues are complex. In either case one is guided by the no-flow and uniform flow solutions. For example, for the cylindrical duct, the no-flow and uniform flow solutions are in the form of Bessel functions of zeroth order. The corresponding eigenvalues indicate the approximate location of the shear flow eigenvalue.

Normally when the eigenvalue is complex it is located by a gradient method as described on page 78 of the book by Betchov and Criminale [6]. The differential equation is integrated twice, once with the starting value, then with a small arbitrary change in the starting value. The direction of the error in the boundary condition is noted and a change in the assumed eigenvalue is made such as to minimize the error. This procedure is repeated. In other words we assume that the error is analytic in β. This is possible only by working with complex numbers throughout.

When the eigenvalue is real it turns out to be easier to use a sweeping method. One starts from the uniform flow value and moves towards the no-flow value. When the sign of the error in the boundary condition changes, the step size $\Delta\beta$ is cut and the location of the eigenvalue is swept until the error is sufficiently small. In the calculations shown here the criterion used is that both the real and imaginary parts of the error in the boundary condition are less than 0·001 for the first six eigenvalues and less than 0·01 for the next five eigenvalues.

Once the eigenvalues and eigenfunctions have been calculated, the amplitude coefficients a_n in the expression (6) for the pressure need to be determined. The values of the eigenfunctions are known at M points between and including $\bar{r}_i$ and $\bar{r}_o$ ($M = 51$ in our case). The a_n are now chosen so as to minimize the sum of the error squared in the pressure profile at M points across the duct passage at $z = 0$. It is easily shown this is achieved when

$$\sum_{k=1}^{M} \sum_{i=0}^{N-1} \{\phi_i(\bar{r}_k)\phi_j(\bar{r}_k)\} a_i = \sum_{k=1}^{M} \hat{p}(\bar{r}_k)\phi_j(\bar{r}_k), \qquad j = 0, 1, \ldots (N-1). \tag{9}$$

These constitute N equations for the N unknowns a_n. The coefficients are then obtained by inverting a complex matrix. Finally the pressure everywhere in the duct is obtained as the real part of (6).

4. RESULTS

The cylindrical and annular geometries will be considered in turn. The axial Mach number profile is taken throughout to be given by a 1/7th power law:

$$\text{cylindrical geometry: } M(\bar{r}) = M_0(1-\bar{r})^{1/7};$$

$$\text{annular geometry: } M(\bar{r}) = M_0\{1-2|\bar{r}_i+0{\cdot}5-\bar{r}|\}^{1/7}.$$

Unless otherwise stated the generating pressure distribution at $z=0$ is uniform, i.e. $p(\bar{r},0,t) = p_0\cos\omega t$ and the walls are hard ($\eta = 0$).

Figures 2(a), 2(b), 2(c) and Tables 1 and 2 refer to sound propagation in a cylindrical duct with a peak flow Mach number of 0·3 and frequency corresponding to $kb = 20$. It is seen from Table 1 that there are seven propagating modes. Figure 2(a) shows the highly distorted lowest

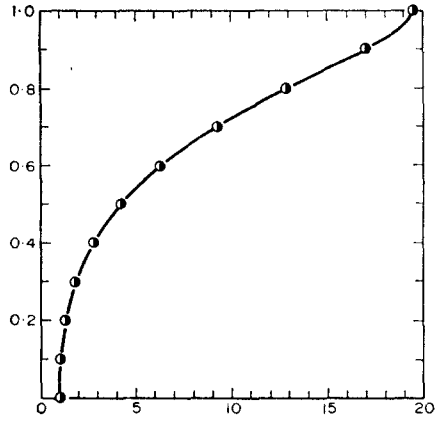

Figure 2(a). The lowest eigenfunction for a hard-walled cylindrical duct, $M_0 = 0{\cdot}3$, $kb = 20$. The real part of ϕ_6 is equal to the imaginary part of ϕ_0.

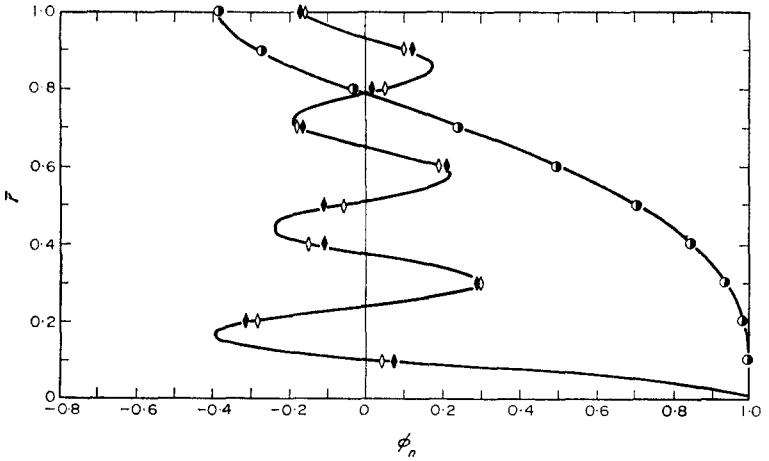

Figure 2(b). The eigenfunction ϕ_1 and the first complex eigenfunction ϕ_7 for a cylindrical duct $\eta = 0$, $M_0 = 0{\cdot}3$, $kb = 20$. ○, ϕ_1; its real part equals its imaginary part; ◇, ϕ_7. The line and open symbols represent the real part, the closed symbols the imaginary part.

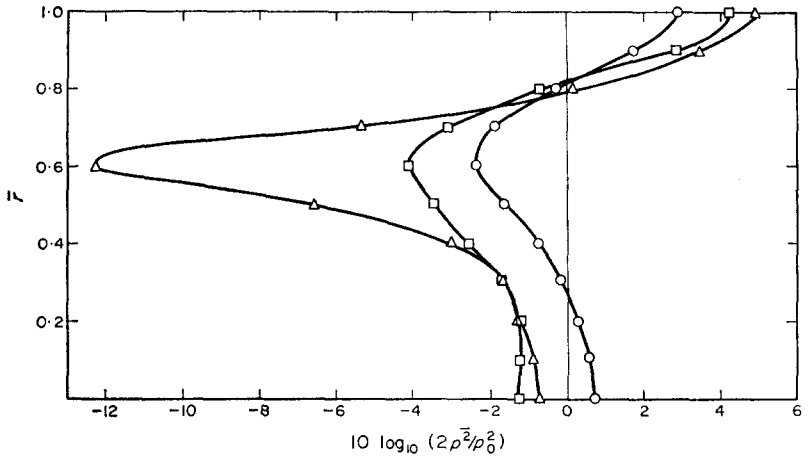

Figure 2(c). Sound pressure profiles in a cylindrical duct, $\eta = 0$, $M_0 = 0{\cdot}3$, $kb = 20$. ○, $z/b = 40$; □, $z/b = 60$; △, $z/b = 80$.

TABLE 1

Eigenvalues and amplitude coefficients for a cylindrical duct, $\eta = 0$, $M_0 = 0{\cdot}3$, $kb = 20$

n	β_n	a_n
0	0·81500	0·03774 − 0·03773i
1	0·76944	0·48128 − 0·48130i
2	0·72751	−0·05956 + 0·05959i
3	0·65329	0·05727 − 0·05731i
4	0·54028	−0·02955 + 0·02955i
5	0·36933	0·02017 − 0·02004i
6	0·06361	−0·01380 + 0·01264i
7	−0·28313 + 0·48807i	0·01096 − 0·01008i
8	−0·28357 + 0·80635i	−0·00762 + 0·00830i
9	−0·28388 + 1·05658i	0·00565 − 0·00684i
10	−0·28410 + 1·27947i	−0·00281 + 0·00355i

TABLE 2

Representation of a uniform source pressure profile at $z = 0$ for a cylindrical duct, $\eta = 0$, $M_0 = 0{\cdot}3$, $kb = 20$

r	Real part of 1	Imaginary part of 1
0·0	0·99942	0·00005
0·1	1·00064	−0·00005
0·2	0·99939	0·00002
0·3	1·00058	0·00001
0·4	0·99946	−0·00006
0·5	1·00048	0·00012
0·6	0·99962	−0·00019
0·7	1·00019	0·00028
0·8	1·00024	−0·00039
0·9	0·99859	0·00050
1·0	1·00443	−0·00050

eigenfunction ϕ_0 while Figure 2(b) shows the next higher eigenfunction ϕ_1 and the first complex eigenfunction ϕ_7. Since the first seven eigenvalues are real the corresponding eigenfunctions have equal real and imaginary parts. The complex eigenvalues, however, lead to eigenfunctions whose real and imaginary parts are unequal. Notice that of the real parts of the eigenfunctions (and also of the complex parts in the hard-walled case) ϕ_0 has no zeros

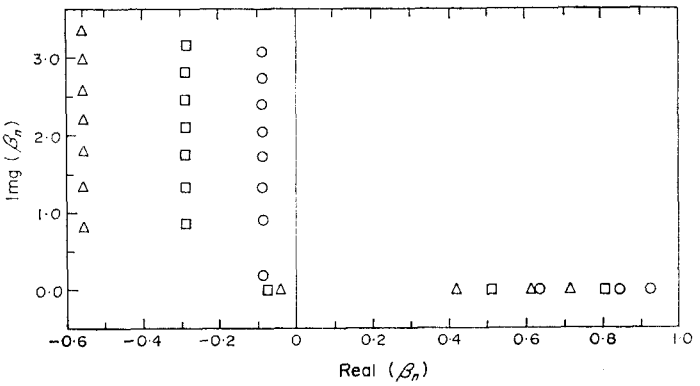

Figure 3(a). Location of the eigenvalues in the complex β plane for a cylindrical duct, $\eta = 0$, $kb = 10$. ○, $M_0 = 0{\cdot}1$; □, $M_0 = 0{\cdot}3$; △, $M_0 = 0{\cdot}5$.

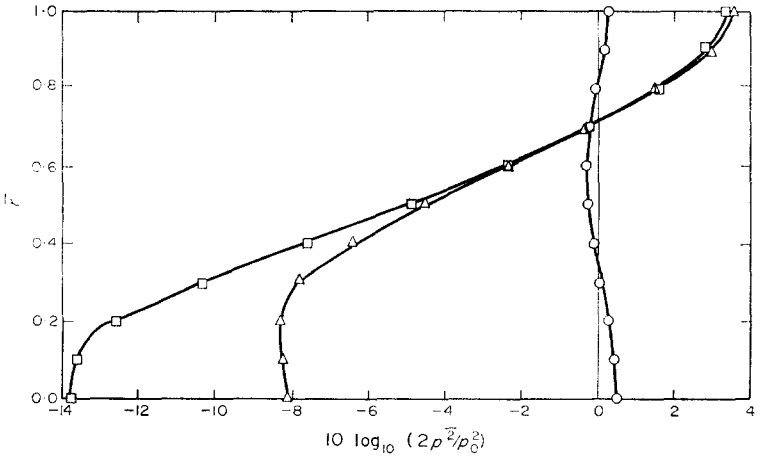

Figure 3(b). The effect of increasing Mach number at a given location in a cylindrical duct, $\eta = 0$, $kb = 10$, $z/b = 100$. ○, $M_0 = 0{\cdot}1$; □, $M_0 = 0{\cdot}3$; △, $M_0 = 0{\cdot}5$.

in the interval, ϕ_1 one and ϕ_7 seven. This illustrates the empirical rule that the number of zeros equals the mode number. It is also typical that only the lowest mode is highly distorted.

Table 1 also shows the amplitude coefficients a_n for this case. The most striking fact is that the largest coefficient is a_1, not a_0, and all the coefficients up to a_7 are of the same order of magnitude as a_0. Thus all the propagating modes are non-negligible; so also is one attenuated one, ϕ_7. However the rest of the coefficients decay rapidly; this is a non-trivial matter from the point of view of practical calculations. Table 2 answers the question of whether the eigenfunctions with these coefficients are able to represent the uniform pressure profile at $z = 0$. Essentially the functions have to represent unity; thus the real parts must add up to one while the imaginary parts should add up to zero over the whole duct cross-section. It is clear that

the representation is excellent. While values at only 11 points across the radius have been shown in Table 2, the error is no worse at 40 other points in the interval.

Figure 2(c) shows the sound pressure patterns in the duct at three axial locations. As a result of our experience with the perturbation calculation, we are not surprised by the complexity of the pressure patterns; all the propagating modes interfere with one another to create standing wave-type patterns. While the peak effect shown is of the order of 16 dB pressure

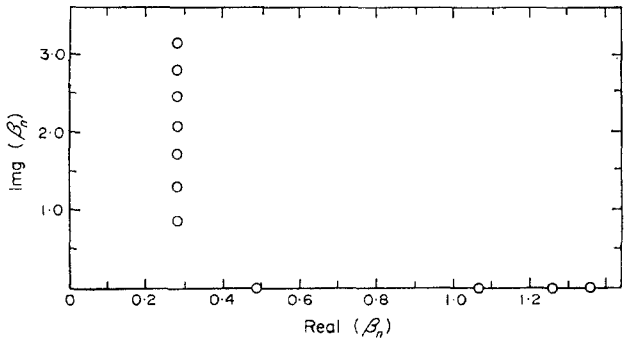

Figure 4(a). Location of the eigenvalues for propagation against the flow in a cylindrical duct, $\eta = 0$, $M_0 = -0{\cdot}3$, $kb = 10$.

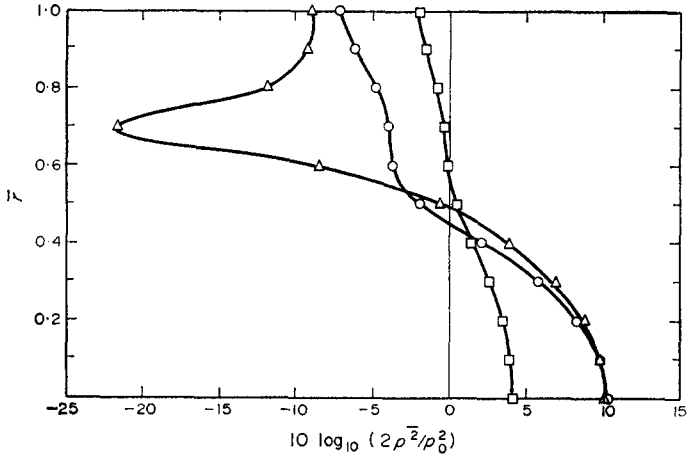

Figure 4(b). Sound pressure profiles for propagation against the flow in a cylindrical duct, $\eta = 0$, $M_0 = -0{\cdot}3$, $kb = 10$. ○, $z/b = 2$; □, $z/b = 20$; △, $z/b = 60$.

difference across the duct, it is mainly due to a fall below the source pressure level rather than a build-up at the wall. This too is typical.

This example (and all the following ones, too) should make clear the futility of trying to infer much about the sound pressure patterns from lowest mode calculations alone. The mode shape and propagation constant are not the only important factors; the amplitude coefficient crucially determines how much of the sound a particular mode carries. As the lowest mode gets more distorted its amplitude decreases; correspondingly the higher modes begin to propagate carrying more of the sound. This saturates the refractive effect. In this example, on the basis of the lowest mode one might expect a 28 dB difference in the sound pressure level between the duct center line and the wall. This is clearly nowhere near the case.

Figures 3(a) and 3(b) show the effect of increasing Mach number at a given frequency. The wavelengths of the modes increase as expected; also one of the higher modes begins to propagate at the higher Mach numbers. As far as the complex eigenvalues are concerned, it is worth noting that the wavelength remains almost constant. This fact can be used to advantage in locating these eigenvalues. From Figure 3(b) it can be seen that the higher Mach numbers lead to accentuated refraction effects but not monotonically; at other z locations the profiles would indeed be different.

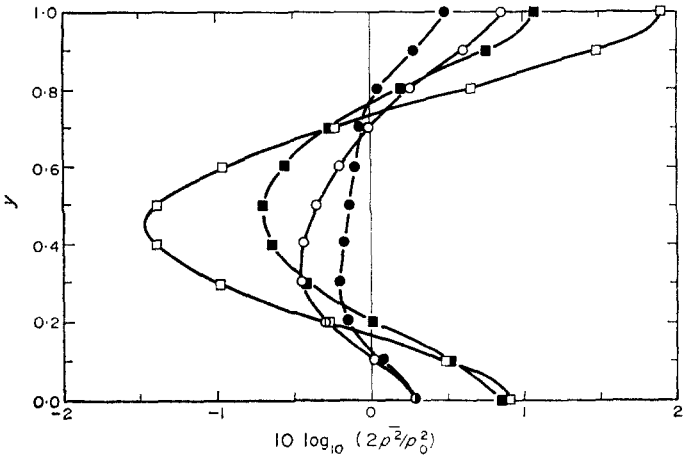

Figure 5. Diametral effects in sound propagation in annular ducts, $\eta = 0$, $M_0 = 0{\cdot}3$, $kb = 10$. The open symbols represent the case $\bar{r}_1 = 2$, the closed ones $\bar{r}_1 = 6$. ○, $z/b = 40$; □, $z/b = 80$.

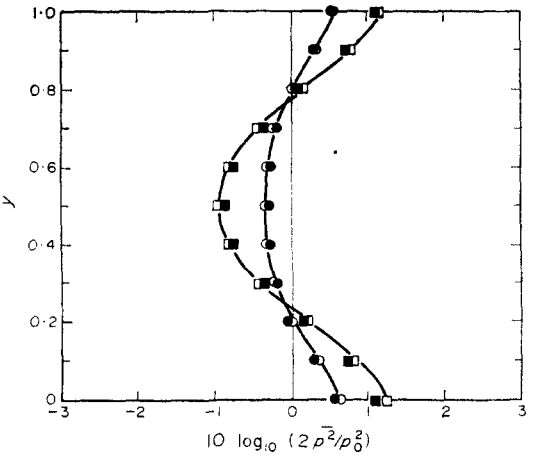

Figure 6. Hard-walled annular duct, $\bar{r}_1 = 20$, $M_0 = 0{\cdot}3$, $kb = 10$. The closed symbols represent corresponding values for a plane two-dimensional duct. ○, $z/b = 60$; □, $z/b = 100$.

When sound has to propagate against the axial flow, the mode wavelengths will tend to get shortened and, moreover, the tendency will be for the sound to channel towards the center of the duct. Figures 4(a) and 4(b) are for an opposing flow Mach number M_0 of 0·3 at a reduced frequency of 10. The channeling effect is striking. For the stations shown the peak build up at the center is 10 dB with a maximum pressure difference across the duct profile of 32 dB. These effects are not insignificant and should be measurable.

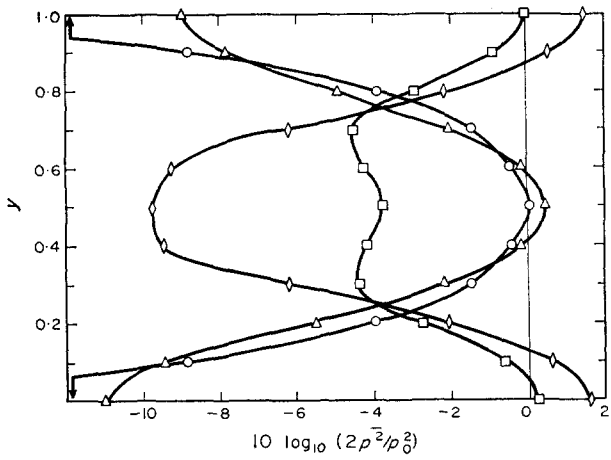

Figure 7. Radiation from a non-uniform source, $p(y,0,t) = 4y(1-y)\, p_0 \cos \omega t$, $\eta = 0$, $M_0 = 0{\cdot}3$, $kb = 10$, $\bar{r}_i = 6$. ○, $z/b = 0$; □, $z/b = 2$; △, $z/b = 20$; ◇, $z/b = 160$.

The remaining figures, Figures 5–10, all deal with annular ducts. The symbol y stands for normalized distance from the inner wall ($y = \bar{r} - \bar{r}_i$). The geometrical effects are clear in that there is no symmetry about the gap centerline ($y = 0{\cdot}5$) even though the axial velocity profile is symmetrical. This asymmetry reduces as the inner radius increases. In the limit of large radius the annular duct should be equivalent to a plane two-dimensional duct. Figure 6 shows that this is indeed the case. The small discrepancy is due to the fact that the plane case has in effect been calculated to greater accuracy. Of the 11 eigenfunctions calculated for the annulus, the 5 odd ones have negligible amplitude, from symmetry requirements. Thus Figure 6 in essence compares the annular case represented with six eigenfunctions to the plane case with eleven. This is the reason for the slight discrepancy.

It should be clear that once the eigenfunctions have been calculated they can be used, if they are complete, to represent any reasonable initial pressure profile. Tables 3 and 4 and Figure 7 show the calculations for an annular duct ($\bar{r}_i = 6$, $M_0 = 0{\cdot}3$, $kb = 10$) with a quadratic

TABLE 3

Eigenvalues and amplitude coefficients for an annular duct with non-uniform source distribution, $\eta = 0$, $\bar{r}_i = 6{\cdot}0$, $M_0 = 0{\cdot}3$, $kb = 10$

n	β_n	a_n
0	0·79293	0·37586 − 0·37463i
1	0·75075	0·00924 − 0·00941i
2	0·57143	−0·25921 + 0·26015i
3	−0·00969	0·00329 − 0·00351i
4	−0·28733 + 0·73219i	−0·05434 + 0·05331i
5	−0·29118 + 1·21721i	0·00158 − 0·00150i
6	−0·29248 + 1·62569i	−0·02600 + 0·02527i
7	−0·29519 + 2·00221i	0·00079 − 0·00072i
8	−0·29567 + 2·36511i	−0·01479 + 0·01359i
9	−0·29768 + 2·71665i	0·00047 − 0·00035i
10	−0·29776 + 3·06414i	−0·00971 + 0·00762i

TABLE 4

Representation of a quadratic source pressure profile at $z = 0$, $\eta = 0$, $\bar{r}_i = 6{\cdot}0$, $M_0 = 0{\cdot}3$, $kb = 10$

y	Real part of $4y(1-y)$	Imaginary part of $4y(1-y)$
0·0	0·05736	−0·00300
0·1	0·36003	0·00188
0·2	0·63388	−0·00076
0·3	0·84806	0·00006
0·4	0·95233	0·00024
0·5	1·00802	−0·00044
0·6	0·95182	0·00030
0·7	0·84685	0·00016
0·8	0·63418	−0·00072
0·9	0·35957	0·00172
1·0	0·05940	−0·00259

sound pressure profile at the generating station $z = 0$:

$$p(y,0,t) = 4p_0\, y(1-y).$$

In this case the amplitudes of the odd eigenfunctions are comparatively much smaller and all the amplitudes decay rapidly. The representation of the initial profile is still good but across the duct the representation is poorest at the walls (Table 4). Going back to the amplitude coefficients, it is apparent that as the odd coefficients are negligible compared to the even ones, the use of more eigenfunctions will in all probability improve the representation, i.e. more even eigenfunctions are needed. From Figure 7 it is clear that even though the initial profile is peaked at the center, the refractive effect causes peaking at the walls at certain axial locations.

As a final example we consider sound propagation in an annular duct ($\bar{r}_i = 2$, $kb = 10$, $M_0 = 0{\cdot}3$) with soft walls. For an admittance $\eta = 0{\cdot}3 + 0{\cdot}1i$, Table 5 shows the eigenvalues

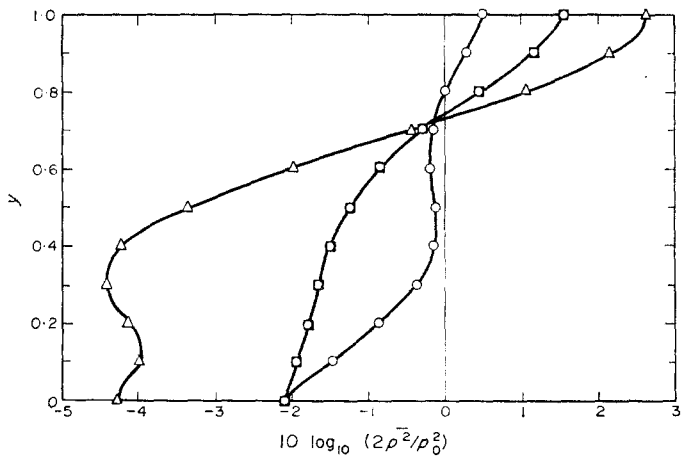

Figure 8. Sound attenuation in a lined annular duct, $\bar{r}_i = 2$, $\eta = 0{\cdot}3 + 0{\cdot}1i$, $M_0 = 0{\cdot}3$, $kb = 10$. ○, $z/b = 0{\cdot}5$; □, $z/b = 1$; △, $z/b = 2$.

and amplitude coefficients. All the modes are now attenuated but the lowest mode suffers the least attenuation. However, since the next two modes have large amplitudes their behavior has a strong influence on the pressure pattern. The representation of the initial profile is still good (Table 6). Figure 8 shows that the pressure decay is extremely non-uniform with an

TABLE 5

Eigenvalues and amplitude coefficients for a soft-walled annular duct, $\eta = 0{\cdot}3 + 0{\cdot}1i$, $\bar{r}_i = 2{\cdot}0$, $M_0 = 0{\cdot}3$, $kb = 10$

n	β_n	a_n
0	$0{\cdot}78698 + 0{\cdot}00400i$	$0{\cdot}46384 - 0{\cdot}00888i$
1	$0{\cdot}73438 + 0{\cdot}02541i$	$0{\cdot}20592 - 0{\cdot}33577i$
2	$0{\cdot}55840 + 0{\cdot}03148i$	$-0{\cdot}10242 - 0{\cdot}03579i$
3	$0{\cdot}14308 + 0{\cdot}07638i$	$-0{\cdot}01083 - 0{\cdot}03755i$
4	$-0{\cdot}23900 + 0{\cdot}74173i$	$-0{\cdot}01561 - 0{\cdot}01683i$
5	$-0{\cdot}26149 + 1{\cdot}21973i$	$-0{\cdot}00616 - 0{\cdot}01418i$
6	$-0{\cdot}26996 + 1{\cdot}62627i$	$-0{\cdot}00738 - 0{\cdot}00788i$
7	$-0{\cdot}27669 + 2{\cdot}00192i$	$-0{\cdot}00347 - 0{\cdot}00718i$
8	$-0{\cdot}27974 + 2{\cdot}36439i$	$-0{\cdot}00356 - 0{\cdot}00491i$
9	$-0{\cdot}28359 + 2{\cdot}71568i$	$-0{\cdot}00181 - 0{\cdot}00432i$
10	$-0{\cdot}28502 + 3{\cdot}06304i$	$-0{\cdot}00200 - 0{\cdot}00348i$

TABLE 6

Representation of a uniform source pressure profile at $z = 0$ *for a soft-walled annular duct,* $\eta = 0{\cdot}3 + 0{\cdot}1i$, $\bar{r}_i = 2{\cdot}0$, $M_0 = 0{\cdot}3$, $kb = 10$

y	Real part of 1	Imaginary part of 1
0·0	0·99339	0·03984
0·1	0·99782	−0·00247
0·2	1·00161	−0·00128
0·3	0·99885	0·00219
0·4	1·00081	−0·00254
0·5	0·99943	0·00267
0·6	1·00040	−0·00273
0·7	0·99963	0·00277
0·8	1·00045	−0·00278
0·9	0·99924	0·00277
1·0	1·00141	−0·00191

actual initial build-up at the upper wall. The geometrical influence is very strong as the inner-wall radius is small. While we have not shown it on the figure, the sound pressure level is negative everywhere within 10 gap widths of the source and decays rapidly with axial distance.

Figures 9 and 10 show the effect of increasing the real part of the wall admittance. It is to be noted that unlike all the other cases shown so far, the imaginary part of the lowest eigen-

function suffers a zero across the interval. Fortunately, the real part does not and so our method of labeling the eigenfunctions still works. This example clearly demonstrates the need for a thorough mathematical study of these eigenfunctions. The comparative effectiveness of the walls in attenuating the sound is shown in Figure 10. The increased admittance is most effective only at the lower wall.

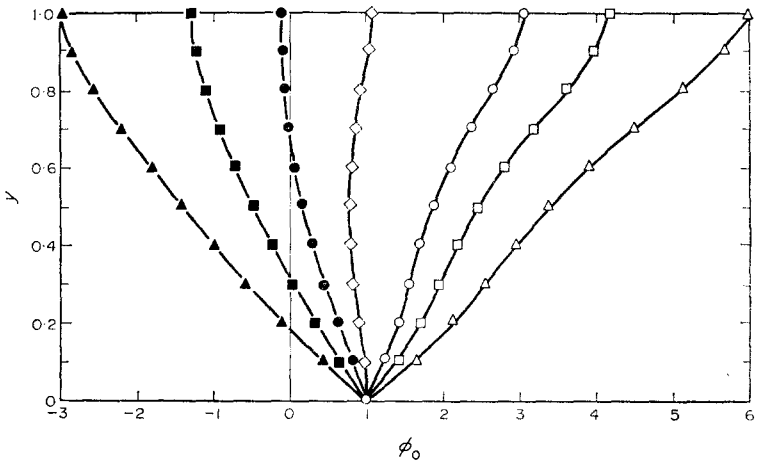

Figure 9. The lowest eigenfunction ϕ_0 for a lined annular duct $\bar{r}_i = 2$, $kb = 10$, $M_0 = 0{\cdot}3$. The open symbols represent the real part of the function and the closed symbol the imaginary part. ◇, $\eta = 0$; ○, $\eta = 0{\cdot}3 + 0{\cdot}1i$; □, $\eta = 0{\cdot}5 + 0{\cdot}1i$; △, $\eta = 0{\cdot}8 + 0{\cdot}1i$.

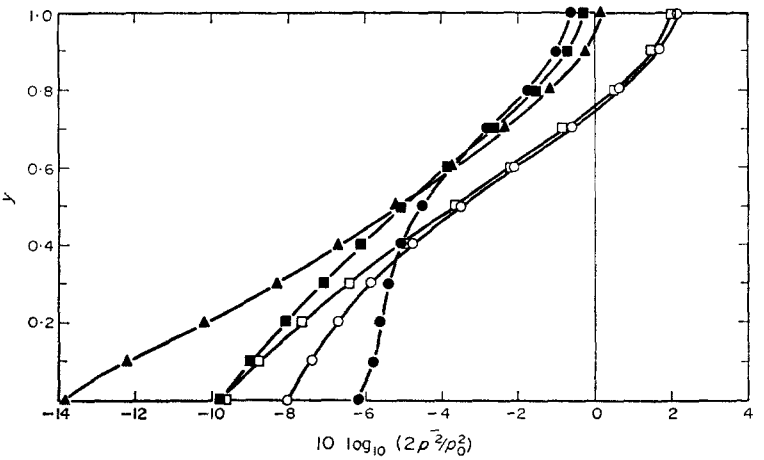

Figure 10. The sound pressure profiles at two axial stations in a lined annular duct, $\bar{r}_i = 2$, $M_0 = 0{\cdot}3$, $kb = 10$. The open symbols refer to $z/b = 5$ and the closed ones to $z/b = 10$. ○, $\eta = 0{\cdot}3 + 0{\cdot}1i$; □, $\eta = 0{\cdot}5 + 0{\cdot}1i$; △, $\eta = 0{\cdot}8 + 0{\cdot}1i$.

All the computations were performed on a UNIVAC 1108 computer. The computing time for a typical calculation, that is for calculating 11 eigenfunctions, the amplitudes and the pressure profile at 12 axial stations, was between 45 seconds and one minute. About 90% of the time goes towards calculating the eigenfunctions. The program was not optimized for time and the integration step size was on the conservative side. The step size for the annular geometry was a constant value of 0·01. The cylindrical geometry with the $\bar{r}^{-1}$ term required more care. The step size used was 0·002 for $0 < \bar{r} < 0{\cdot}1$ and 0·02 for $0{\cdot}1 < \bar{r} < 1{\cdot}0$.

5. CONCLUDING REMARKS

We have attempted to show here how calculations of acoustic refraction and attenuation in cylindrical and annular ducts may be made. Detailed parametric investigations to determine the effects of frequency, admittance, annular radius and Mach number on the propagation and attenuation characteristics would probably best be carried out independently for particular applications. The present calculations, however, reaffirm the importance of considering the complete boundary value problem; lowest mode calculations are in themselves misleading.

In surveying the work done in this area to date, two profitable avenues of future research suggest themselves. Detailed mathematical investigations of the non-linear eigenvalue problems of acoustic refraction might lead to theorems on the nature of the eigenvalues and eigenfunctions and on their completeness. The present calculations indicate that the eigenfunctions are in all probability complete. However, it would be preferable not to have to rely on faith and intuition! Secondly, there is a need for a thorough investigation of the boundary conditions at absorbent walls. At present there is considerable doubt about the adequacy of a simple condition such as (5a), even in the absence of slip at the wall. The admittance might very well be a function of frequency, geometry, etc; or a totally different boundary condition might be more appropriate. Finally, of course, only detailed experiments can settle this question.

REFERENCES

1. D. C. PRIDMORE-BROWN 1958 *Journal of Fluid Mechanics* **4**, 393–406. Sound propagation in a fluid flowing through an attenuating duct.
2. P. MUNGUR and G. M. L. GLADWELL 1969 *Journal of Sound and Vibration* **9**, 28–48. Acoustic wave propagation in a sheared fluid contained in a duct.
3. P. MUNGUR and H. E. PLUMBLEE 1969 *National Aeronautics and Space Administration, Washington, D.C. SP-207*. Propagation and attenuation of sound in a soft walled annular duct containing a sheared flow.
4. P. N. SHANKAR 1971 *Journal of Fluid Mechanics* **47**, 81–91. On acoustic refraction by duct shear layers.
5. P. N. SHANKAR 1972 *Journal of Sound and Vibration* **22**, 221–232. Sound propagation in duct shear layers.
6. R. BETCHOV and W. O. CRIMINALE 1967 *Stability of parallel flows*. New York: Academic Press.